Optics Communications 285 (2012) 393–401

Contents lists available at SciVerse ScienceDirect

Optics Communications

journal homepage: www.elsevier.com/locate/optcom

Analysis of optical polarization modulation systems through the Pancharatnam connection

José Luis Martínez-Fuentes *, Jorge Albero, Ignacio Moreno

Departamento de Ciencia de Materiales, Óptica y Tecnología Electrónica, Universidad Miguel Hernández, 03202 Elche, Spain

ARTICLE INFO

Article history:
Received 15 August 2011
Received in revised form 27 September 2011
Accepted 3 October 2011
Available online 20 October 2011

OCIS codes:
(260.5430) Polarization
(350.5030) Phase
(060.5060) Phase modulation
(350.1370) Berry's phase

Keywords:
Complex modulation
Pancharatnam's connection
Liquid Crystal displays

ABSTRACT

We present a geometrical analysis on the Poincaré sphere of the complex (amplitude and phase) response of polarization modulation systems. The proposed method can be applied to analyze non-cyclic polarization changes and, in particular, the phase is evaluated through the geometric Pancharatnam–Berry phase and the Pancharatnam connection between the initial and the final state. The method can be very useful to analyze and intuitively understand the complex modulation mechanism in polarization modulation devices such as liquid crystal displays.

1. Introduction

In 1956 Pancharatnam [1] defined the idea of relative phase between two polarization states, and established a criterion for which two different polarization states are in phase, the so-called Pancharatnam connection. These important results went unnoticed until Berry related the Pancharatnam geometric phase and the geometric phase of slowly varying (adiabatic) cyclic quantum systems for 1/2 spin particles [2]. Since then, the phase gained when a sequence of transformations are performed onto the state of polarization along a closed loop of geodesic arcs (parallel transport) on the Poincaré sphere, the so-called geometric Pancharatnam–Berry phase, has been extensively analyzed [3–5] and applied for the design of systems to manipulate the state of polarization [6,7].

However, in some important practical systems, the polarization transformations either follow non-geodesic trajectories (this is in general the case when traversing wave plates), or non-closed loops on the Poincaré sphere. The first situation has been usually solved by decomposing the total phase gain into a geometrical part (half the area limited by the closed trajectory on the sphere) and a dynamical phase term [8,9], which can be regarded as a phase term with no shape identification on the sphere. However, a methodology to geometrically derive the overall phase gained by the light beam in closed loops that include traversing wave plates was developed by Courtial in ref [10]. Recently, the methodology of Courtial has been revisited by Kurzynowski et al. [11] and also independently derived by Gutierrez-Vega [12]. Van Dijk et al. also proposed a methodology to geometrically evaluate the phase of non-closed loop polarization transformations [13,14].

All these works show the usefulness of developing geometrical methods based on the Poincaré sphere representation to evaluate the phase gained by a light beam traversing polarization optical systems. This can be especially useful to analyze the complex (amplitude and phase) modulation in polarization optoelectronic modulators, including devices like liquid-crystal, electro-optic or elasto-optic modulators. All these devices can be considered in general as elliptical wave plates, i.e., a waveplate whose eigenvectors are elliptical states instead of linear ones. In such devices one or more physical parameters (the phase shift and / or its eigenvectors) can be modulated through an applied voltage. For instance, parallel aligned liquid crystal devices (PAL-LCD) show a voltage dependence of the eigenphases, while they maintain fixed eigenvectors [15]. Ferroelectric liquid crystal devices (FLCD), on the contrary, respond to a binary bipolar voltage with a variation in the orientation of the eigenstates, while they maintain fixed eigenphases [16]. The most common device, the twisted nematic liquid crystal display (TN-LCD), presents variations with voltage in both the eigenphases and the eigenstates [17,18].

* Corresponding author. Tel.: +34 966658639.
E-mail address: jose.martinez@umh.es (J.L. Martínez-Fuentes).

0030-4018/$ – see front matter © 2011 Elsevier B.V. All rights reserved.
doi:10.1016/j.optcom.2011.10.016

In all cases, the modulator is typically illuminated with a specific elliptical polarization. If the devices are pixelated, they can be employed to create non-uniform polarization light beams [19]. Nevertheless, in general, the light emerging from the modulator is projected onto an elliptical analyzer, i.e., a polarizer whose transmission state is an elliptical state, which is commonly made of a quarter wave plate followed by a linear polarizer, to produce a desired complex modulation (typically a phase only modulation) [20]. The configuration of these external polarization elements (polarizers and fixed wave plates) determines the complex modulation produced as a function of the applied voltage. For instance, the range of the phase modulation can be dramatically increased in TN-LCD when a proper elliptical polarization configuration is selected [17]. Usually, the identification of the overall amplitude and phase modulation is performed using the Jones theory. However, although the Poincaré sphere has been employed to analyze the polarization transformations upon modulation [16,18,20], the geometrical Pancharatnam–Berry approach has not been applied to understand, analyze or predict the mechanisms involved in phase modulation of such modulators.

In this work we present a procedure to describe the complex modulation achieved by polarization modulators based on the application of the geometrical phase approach. For that purpose, we geometrically analyze the two polarization transformations produced on such systems: 1) the transformation induced by the modulator, which requires accounting for the geometrical Pancharatnam–Berry phase, for the dynamical phase, but also for an additional phase term accounting for the non-closed loop among the initial state and the state emerging from the modulator, and 2) the projection onto the state transmitted by the final elliptical analyzer, for which the Pancharatnam connection can be directly applied. In order to analyze such transformations we apply specific simple spherical quadrangles defined on the Poincaré sphere, which can be applied to evaluate both types of transformation.

For that purpose, in Section 2 we review the Pancharatman's connection to project one polarization state onto another, and we develop a simple spherical quadrangle to geometrically visualize the corresponding phase gain. Then, in Section 3 we analyze the phase gain when the light beam traverses a general elliptical wave plate, creating a non-closed loop, and we show that an additional Pancharatman connection phase term must be added to the usual dynamical and geometrical phase terms employed when closed loops are considered. In Section 4 we present how to combine both situations (passage through a general elliptical wave plate, and projection of the emerging state onto an arbitrary elliptical analyzer), and we derive geometrical shapes that permit to geometrically evaluate the overall complex modulation. Finally, in Section 5 we introduce the application of this method to evaluate the modulation produced by a parallel aligned nematic liquid crystal display in various polarization configurations. Experimental results that verify the presented results are included.

2. Pancharatnam connection through spherical quadrangles

A natural way to represent any polarization state, directly related to the Poincaré sphere, is the azimuth–ellipticity notation. A unitary polarization state $|e\rangle \equiv |\theta,\varepsilon\rangle$, defined by its azimuth (θ) and ellipticity (ε) angles, can be expressed in terms of the corresponding Jones vector as:

$$|e\rangle = |\theta,\varepsilon\rangle = \mathbf{R}(-\theta)\begin{bmatrix}\cos(\varepsilon)\\ i\sin(\varepsilon)\end{bmatrix}, \tag{1}$$

where R is the 2×2 rotation matrix

$$\mathbf{R}(\theta) = \begin{bmatrix}\cos(\theta) & \sin(\theta)\\ -\sin(\theta) & \cos(\theta)\end{bmatrix}. \tag{2}$$

The corresponding unitary Stokes vector is expressed as:

$$\mathbf{S}(\theta,\varepsilon) = \begin{bmatrix}\cos(2\varepsilon)\cos(2\theta)\\ \cos(2\varepsilon)\sin(2\theta)\\ \sin(2\varepsilon)\end{bmatrix}, \tag{3}$$

which directly defines the polarization state coordinates on the Poincaré sphere, being $(2\theta, 2\varepsilon)$ the longitude and latitude angles.

Next, let us consider the projection p_{ab} of a state $|a\rangle = |\theta_a,\varepsilon_a\rangle$ onto a state $|b\rangle = |\theta_b,\varepsilon_b\rangle$, both being unitary states described by a Jones vector in the form of Eq. (1), i.e., without additional external phases. The result of this projection can be written as the polarization state $|B\rangle = |b\rangle\langle b|a\rangle$, where the scalar term $p_{ab} = \langle b|a\rangle$ can be calculated as:

$$\begin{aligned} p_{ab} &= \cos(\theta_a-\theta_b)\cos(\varepsilon_a-\varepsilon_b) + i\sin(\theta_a-\theta_b)\sin(\varepsilon_a+\varepsilon_b)\\ &= \cos\left(\frac{\gamma_{ab}}{2}\right)\exp(i\varphi_{ab}) \end{aligned} \tag{4}$$

where $\theta_{a/b}$ and $\varepsilon_{a/b}$ denote the corresponding azimuth and ellipticity angles, and γ_{ab}, φ_{ab} are angular magnitudes which define the amplitude and the phase for this projection. The intensity of the projection is given by:

$$i_{ab} = |\langle b|a\rangle|^2 = \cos^2\left(\frac{\gamma_{ab}}{2}\right) = \frac{1}{2}(1+\mathbf{S}_a\cdot\mathbf{S}_b), \tag{5}$$

being S_a and S_b the Stokes vectors corresponding to $|a\rangle$ and $|b\rangle$. From this expression, γ_{ab} gets its meaning as the great arc on the Poincaré sphere joining states $|a\rangle$ and $|b\rangle$. The phase $\varphi_{ab} = \arg\{p_{ab}\}$, i.e., their Pancharatnam connection, can be directly derived from Eqs. (4)–(5) to be

$$\varphi_{ab} = \arctan\left(\tan(\theta_a-\theta_b)\frac{\sin(\varepsilon_a+\varepsilon_b)}{\cos(\varepsilon_a-\varepsilon_b)}\right). \tag{6}$$

This shows that, for the chosen representation of the polarization states (Eq. (1)), only those states having either the same azimuth or opposite ellipticity will be in phase to each other.

According to the geometric phase concept, the phase gained in a closed loop along geodesic arcs (parallel transport) is given by half the solid angle defined by the closed trajectory. Therefore, a construction like that in Fig. 1(a) can be done, where an spherical quadrangle is defined by the states $|a\rangle$, $|b\rangle$, and two other linear states $|a'\rangle = |\theta_a,0\rangle$ and $|b'\rangle = |\theta_b,0\rangle$ with the same azimuth as $|a\rangle$ and $|b\rangle$, respectively. The closed trajectory $|a\rangle\to|b\rangle\to|b'\rangle\to|a'\rangle\to|a\rangle$ along geodesic arcs defines a solid angle $\Omega_{ab}\equiv\Omega_{abb'a'}$. Arcs $|b\rangle\to|b'\rangle$ and $|a'\rangle\to|a\rangle$ correspond to transformations without change in the azimuth, and arc $|b'\rangle\to|a'\rangle$ corresponds to a transformation with zero ellipticity. Thus, according to Eq. (6), they do not introduce any phase upon projection. Having into account Pancharatnam–Berry theory, it is directly concluded that the phase φ_{ab} must coincide with minus half the solid angle Ω_{ab} of the spherical quadrangle defined in Fig. 1(a). Thus, the projection p_{ab} can be written as

$$p_{ab} = \langle b|a\rangle = \cos\left(\frac{\gamma_{ab}}{2}\right)\exp\left(-i\frac{\Omega_{ab}}{2}\right). \tag{7}$$

The following sign criteria for Ω_{ab} can be directly concluded from Eq. (6): if the sequence $|a\rangle\to|b\rangle\to|b'\rangle\to|a'\rangle\to|a\rangle$ is followed counterclockwise, then Ω_{ab} is positive; if this sequence is followed clockwise, then Ω_{ab} is negative. Also note that the projection in opposite sense has opposite sign solid angle, i.e., $\Omega_{ba} = -\Omega_{ab}$.

If the two states lie in opposite hemispheres of the Poincaré sphere, the above spherical quadrangle degenerates into two spherical triangles, as shown in Fig. 1(b). Now, the solid angle Ω_{ab} can be viewed as the sum of the two angles $\Omega_{aca'}$ and $\Omega_{bb'c}$ corresponding to the two triangles in Fig. 1(b), being $|c\rangle$ the state obtained by the intersection between the great circle joining $|a\rangle$ and $|b\rangle$, and the

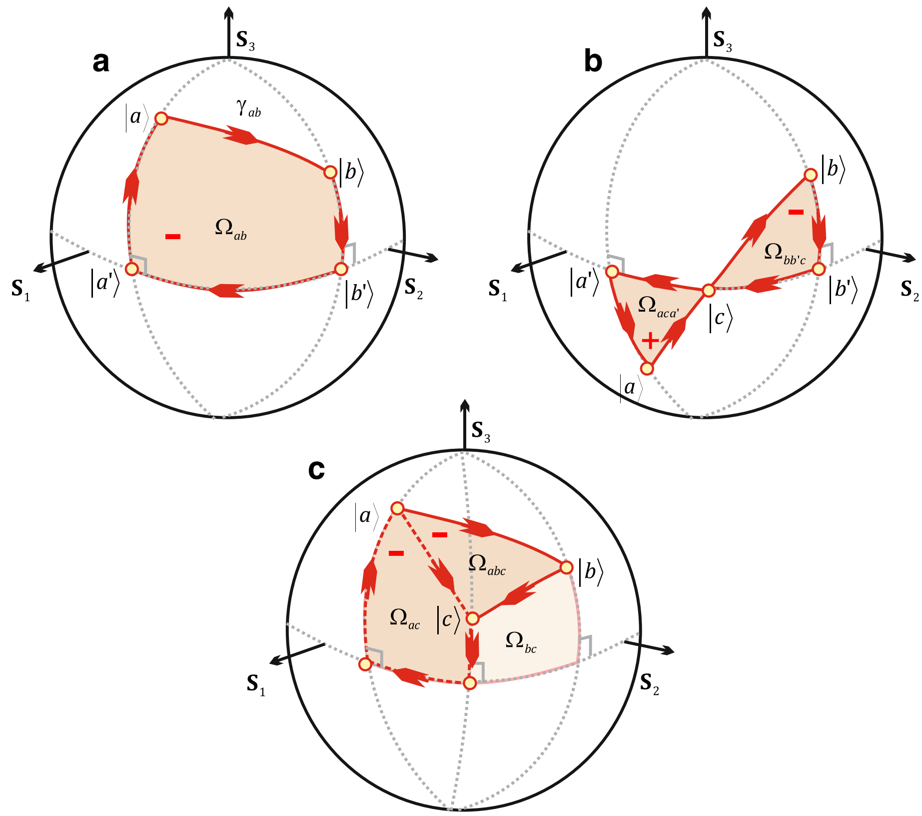

Fig. 1. (a) Spherical quadrangle Ω_{ab} to calculate the projection $\langle b|a\rangle$. (b) Two equivalent spherical triangles to calculate $\langle b|a\rangle$when $|a\rangle$ and $|b\rangle$ lie in opposite hemispheres. (c) Spherical triangle Ω_{abc} and spherical quadrangle Ω_{ac} useful to calculate the phase of the non-closed loop of projections $\langle c|b\rangle\langle b|a\rangle$.

equator. The above mentioned sign criteria must be applied to each triangle separately. Therefore, in the case shown in Fig. 1(b) $\Omega_{\text{aca'}}$ is positive while $\Omega_{\text{bb'c}}$ is negative.

Finally, let us note that, according to the Pancharatnam–Berry phase theorem, if the input state $|a\rangle$ is first projected onto $|b\rangle$, then onto a third state $|c\rangle$, and finally back to the initial state $|a\rangle$, the total gained phase shift is given by minus half the solid angle Ω_{abc} of the triangle defined by these three states and the geodesic arcs joining them. Note that this solid angle can be composed by the sum of the signed solid angles of each projection, each one represented by a solid spherical quadrangle as $\Omega_{\text{abc}}=\Omega_{\text{ab}}+\Omega_{\text{bc}}+\Omega_{\text{ca}}$. Equivalently, if the initial state $|a\rangle$ is projected onto the final state $|c\rangle$ through an intermediate state $|b\rangle$, therefore producing a non-closed loop, the solid angles related to these transformation follow

$$\Omega_{\text{ab}}+\Omega_{\text{bc}}=\Omega_{\text{abc}}+\Omega_{\text{ac}} \tag{8}$$

Therefore, the phase of non-closed loop of projections $|a\rangle\rightarrow|b\rangle\rightarrow|c\rangle$ is equal to the Pancharatnam–Berry phase related to the closed loop $|a\rangle\rightarrow|b\rangle\rightarrow|c\rangle\rightarrow|a\rangle$, plus the phase of the Pancharatnam connection related to the projection $|a\rangle\rightarrow|c\rangle$. This is illustrated in Fig. 1(c), where the solid angles Ω_{abc} and Ω_{ac} are both negative for this case. We will make use of this result in the next sections, when dealing with the transformation through wave plates.

3. Phase gain through a wave plate

We next study how to geometrically analyze the phase gained by a polarization state $|a\rangle$ which traverses an elliptical retarder wave plate, i.e., a non-absorbing polarization device characterized by a unitary Jones matrix T, i.e., $T^{\dagger}=T^{-1}$, being † the transposed complex-conjugate operator. The matrix of this device can be written as:

$$\mathbf{T}=\exp(i\varphi_1)|1\rangle\langle 1|+\exp(i\varphi_2)|2\rangle\langle 2|, \tag{9}$$

where $|1\rangle$ and $|2\rangle$ denote the two eigenvectors or neutral axes of the wave plate (those polarization states which pass through the wave plate unaltered except for its eigenphase exponential term). Apart from this, φ_1 and φ_2 are the corresponding eigenphases. This previous equation can be written in terms of the mean phase shift $2\overline{\varphi}=(\varphi_2+\varphi_1)=\arg(\det(\mathbf{T}))$ and the retardance $2\omega=(\varphi_2-\varphi_1)$ as

$$\mathbf{T}=\exp(i\overline{\varphi})\{\exp(-i\omega)|1\rangle\langle 1|+\exp(+i\omega)|2\rangle\langle 2|\} \tag{10}$$

The phase shift $\overline{\varphi}$ corresponds to the mean phase component acquired when a light beam traverses the wave plate, while the matrix inside the braces in Eq. (10) corresponds to a SU(2) group transformation [3], i.e. a 2×2 unitary matrix with a determinant equal to one.

It is very well known that the action of a retarder on the Poincaré sphere is to produce a rotation of 2ω around the axis defined by its eigenstates $|1\rangle$ and $|2\rangle$. This is illustrated in Fig. 2(a), where the input state $|a\rangle$ is transformed into the state $|B\rangle=\mathbf{T}|a\rangle$. The lune defined by the states $|1\rangle$, $|2\rangle$, $|a\rangle$ and $|B\rangle$ has a solid angle 4ω. According to the selected sign criteria, ω is positive if the rotation seen from axis $|1\rangle$ is counterclockwise.

The trajectory corresponding to the transformation induced by the wave plate (black solid line in Fig. 2(a)) is a non-geodesic opened arc. Therefore $|B\rangle$ is not in phase with $|a\rangle$. Thus, it must be expressed as $|B\rangle=\exp(i\varphi_{\mathbf{T}:a\rightarrow b})|b\rangle$, where now $|b\rangle$ takes the form

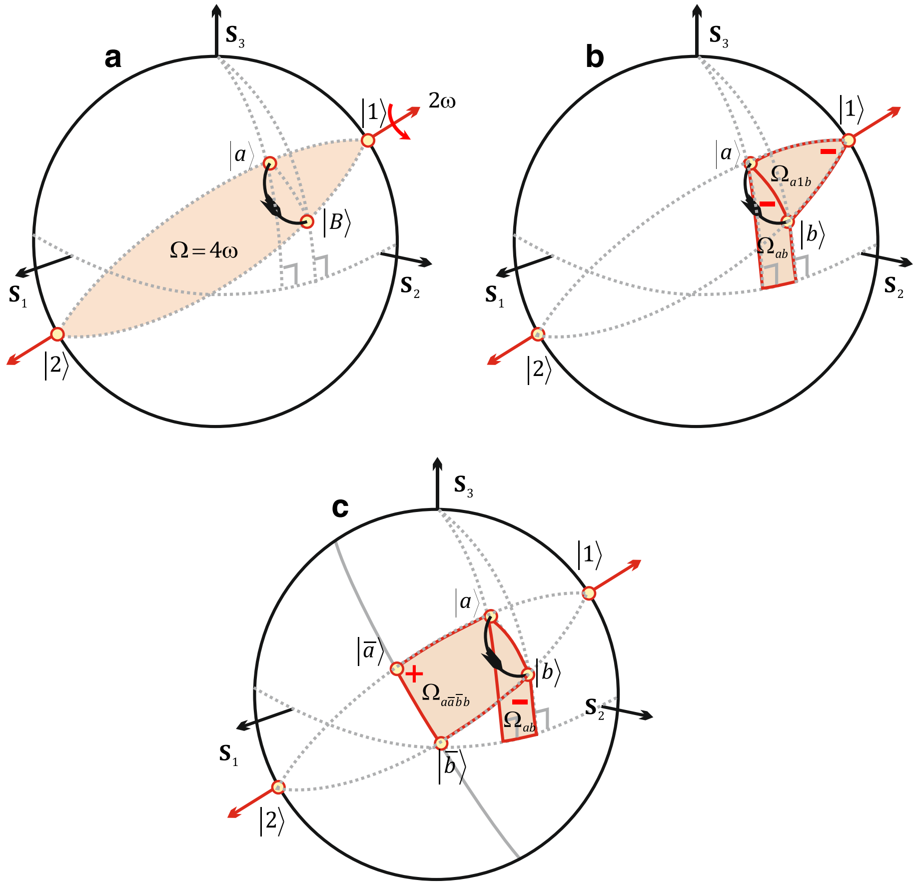

Fig. 2. (a) Rotation in the Poincaré sphere induced by an elliptical wave plate with eigenvectors $|1\rangle$ and $|2\rangle$ and retardance 2ω. (b, c) Alternative spherical shapes useful to geometrically calculate the phase gain $\varphi_{\mathbf{T}:a\to b}$: (b) Spherical triangle Ω_{a1b} and spherical quadrangle Ω_{ab}(this construction requires adding the eigenphase ϕ_1 of the selected eigenvector; Eq. (13)), (c) Spherical quadrangles $\Omega_{a\bar{a}\bar{b}b}$ and Ω_{ab}(this construction requires adding the average eigenphase $\overline{\varphi}$; Eq. (14)).

of Eq. (1). Following Courtial [9], this phase can be calculated by projecting the output state $|B\rangle$ onto one of the two orthogonal eigenvectors. Let us calculate $p_{Bn} = \langle n|B\rangle = \exp(i\varphi_{\mathbf{T}:a\to b})\langle n|b\rangle$ with $|n\rangle$, $n = 1,2$, the two wave plate eigenvectors. By direct application of Eq. (9) and because the eigenvectors satisfy that $\mathbf{T}|n\rangle = \exp(i\varphi_n)|n\rangle$, and $\langle 1|2\rangle = \langle 2|1\rangle = 0$, it is directly derived that $\langle n|B\rangle = \langle n|\mathbf{T}|a\rangle = \exp(i\varphi_n)\langle n|a\rangle$. Joining these two results directly leads to the following expression

$$\exp(i\varphi_{\mathbf{T}:a\to b}) = \exp(i\varphi_1)\frac{\langle 1|a\rangle}{\langle 1|b\rangle} = \exp(i\varphi_2)\frac{\langle 2|a\rangle}{\langle 2|b\rangle} \tag{11}$$

Since the transformation of $|a\rangle$ into $|b\rangle$ by the wave plate keeps the angle γ to the selected eigenvector state, $\gamma_{\mathrm{an}} = \gamma_{\mathrm{bn}}$, the previous equation can be written using only the phase terms as $\exp(i\varphi_{\mathbf{T}:a\to b}) = \exp(i\varphi_n)\exp(-i\Omega_{an}/2)\exp(+i\Omega_{bn}/2)$, or in other terms

$$\varphi_{\mathbf{T}:\mathrm{a}\to\mathrm{b}} = \varphi_1 + \frac{\Omega_{\mathrm{b}1} - \Omega_{\mathrm{a}1}}{2} = \varphi_2 + \frac{\Omega_{\mathrm{b}2} - \Omega_{\mathrm{a}2}}{2}. \tag{12}$$

This result implies that the phase $\varphi_{\mathbf{T}:a\to b}$, gained by the non-geodesic circular movement from state $|a\rangle$ to $|B\rangle$, is equal to the phase of the considered eigenvector, plus the phase difference between the projections of the input $|a\rangle$ and output $|b\rangle$ states onto the selected eigenvector. Taking into account the decomposition in Eq. (8), this result can also be written as

$$\varphi_{\mathbf{T}:a\to b} = \varphi_1 - \frac{\Omega_{a1b}}{2} - \frac{\Omega_{ab}}{2} = \varphi_2 - \frac{\Omega_{a2b}}{2} - \frac{\Omega_{ab}}{2} \tag{13}$$

This alternative expression shows that $\varphi_{\mathbf{T}:a\to b}$ can also be calculated as the sum of three contributions: 1) the phase ϕ_n of the considered eigenvector $|n\rangle$, 2) the Pancharatnam–Berry phase corresponding to the closed loop $|a\rangle\to|n\rangle\to|b\rangle\to|a\rangle$, and 3) the phase of the Pancharatnam connection $|a\rangle\to|b\rangle$. Fig. 2(b) shows an example where the first eigenvector is considered, and where the spherical triangle defined by states $|a\rangle$, $|1\rangle$ and $|b\rangle$, with area Ω_{a1b} (negative in this case), and the spherical quadrangle with area Ω_{ab}(also negative in this case) have been marked.

If the two previous relations in Eq. (13) are averaged, the phase $\varphi_{\mathbf{T}:a\to b}$ can also be calculated as

$$\varphi_{\mathbf{T}:a\to b} = \overline{\varphi} - \frac{\Omega_{a\bar{a}\bar{b}b}}{2} - \frac{\Omega_{ab}}{2}, \tag{14}$$

where $\Omega_{a\bar{a}\bar{b}b} = \frac{1}{2}(\Omega_{a1b} + \Omega_{a2b}) = 2\omega - \Omega_{b1a}$ is the solid angle in the spherical quadrangle defined by states $|a\rangle$,$|b\rangle$, $|\bar{a}\rangle$ and $|\bar{b}\rangle$ as shown in Fig. 2(c). Note that this spherical quadrangle is a portion of half the lune of angle 2ω defined by states $|1\rangle$, $|\bar{a}\rangle$ and $|\bar{b}\rangle$. Also note that the great arc passing through $|\bar{a}\rangle$ and $|\bar{b}\rangle$ defines a great circle, which is perpendicular to the axis joining the eigenstates $|1\rangle$ and $|2\rangle$.

Eq. (14) shows that the phase shift $\varphi_{\mathbf{T}:a\to b}$ can be split into three components as $\varphi_{\mathbf{T}:a\to b} = \varphi^D + \varphi^G + \varphi^{PC}$, where $\varphi^D = \overline{\varphi}$ is a phase component with no geometrical identification (which could be regarded as a dynamical phase term in this particular decomposition), while $\varphi^G = -\Omega_{a\bar{a}\bar{b}b}/2$ denotes a geometrical phase term. Note that these two components have been recently identified in refs. [10,11]. However, the additional component $\varphi^{PC} = -\Omega_{ab}/2$ must be added, corresponding to the Pancharatnam connection from $|a\rangle$ to $|b\rangle$. If the loop on the Poincaré sphere is finally closed by projecting $|b\rangle$ back onto $|a\rangle$, an additional Pancharatnam connection phase term $\varphi_{ba} = \arg(\langle a|b\rangle) = -\Omega_{ba}/2$ must be added, which exactly cancels φ^{PC}. This is the case in the typical experiment dealing with the geometrical phase, where the polarization optical system is included in one arm of an interferometer, and the phase of the emerging state is compared to the phase of the initial state [8].

However, the third term in Eq. (14), $\varphi^{PC} = -\Omega_{ab}/2$ cannot be ignored in optical modulator systems, where the final state is not projected in general onto the initial one, and becomes very important to explain the phase modulation characteristics of the devices.

An additional observation regarding the meaning of Eq. (14) can be done. It splits the origin of the phase gain into two terms. On one hand, the mean phase $\overline{\varphi}$, which has no evident interpretation on the sphere. On the other hand, the geometrical terms $\varphi^G = -\Omega_{a\bar{a}\bar{b}b}/2$ and $\varphi^{PC} = -\Omega_{ab}/2$, which are direct consequence of the SU(2) transformation previously alluded to in Eq. (10). This verifies that the phase gain produced by any SU (2) transformation (2×2 unitary matrix with 1 determinant) can be identified by means of two simple geometrical shapes on the sphere.

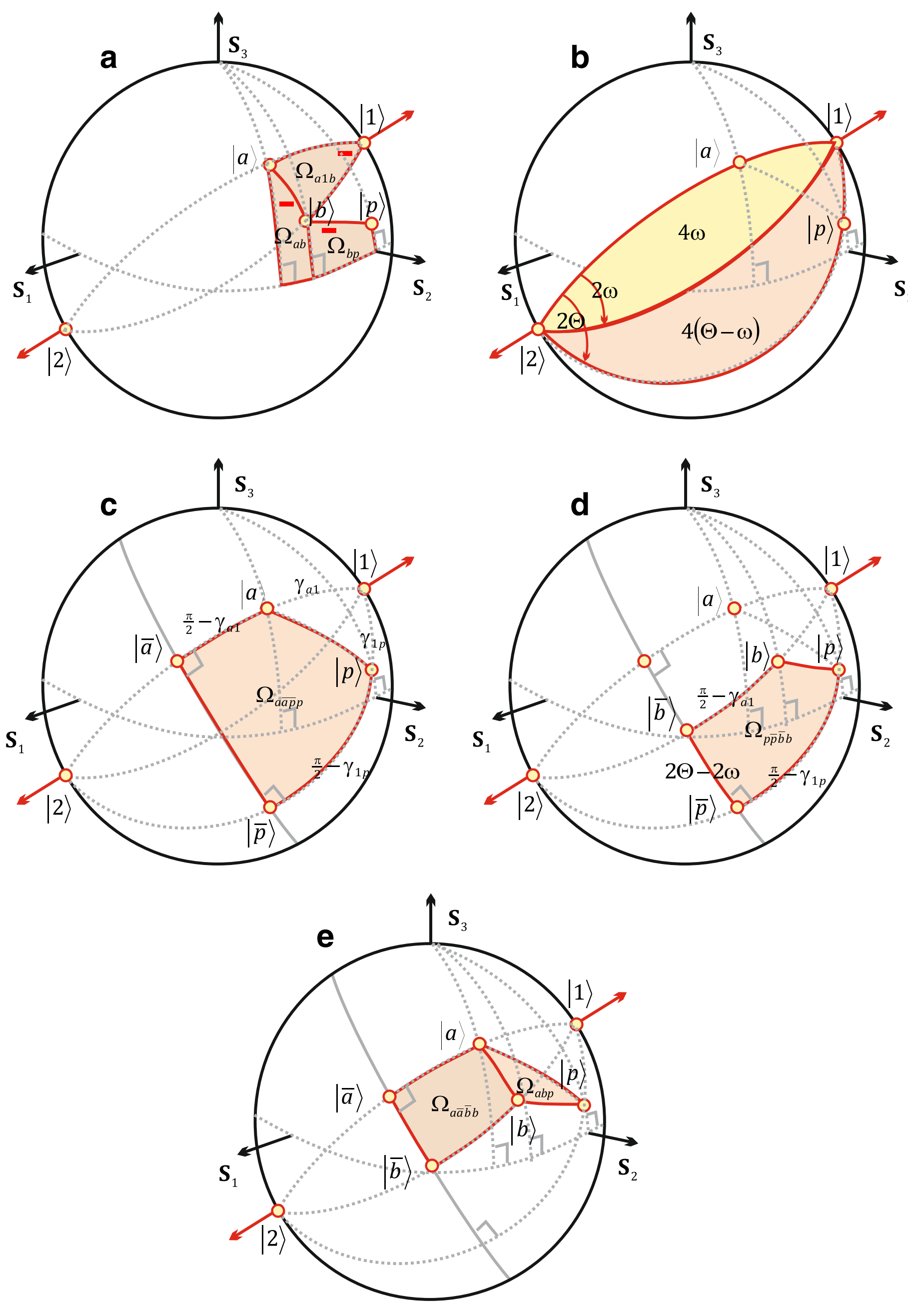

Fig. 3. Spherical shapes useful to geometrically calculate the complex modulation m: (a) Spherical triangle Ω_{a1p} and spherical quadrangle Ω_{ap}, (b) spherical lunes with areas 4Θ and 4ω and their difference, (c) spherical quadrangle $\Omega_{a\bar{a}\bar{p}p}$, (d) spherical quadrangle $\Omega_{p\bar{p}\bar{b}b}$ and (e) spherical triangle Ω_{abp} and spherical quadrangle $\Omega_{a\bar{a}\bar{b}b}$.

4. Projection onto a final analyzer

Let us now consider the projection of the state $|B\rangle = \mathbf{T}|a\rangle = \exp(i\varphi_{\mathbf{T}a\to b})|b\rangle$ emerging from the modulator onto an arbitrary final elliptical analyzer, represented by the state $|p\rangle$. This complete process is visualized in Fig. 3(a), and the final projection leads to an additional complex modulation term $\langle p|b\rangle = \cos(\gamma_{bp}/2)\exp(-i\Omega_{bp}/2)$. Thus, the total complex modulation m provided by the modulator is given by

$$\begin{aligned} m &= \langle p|B\rangle = \langle p|\mathbf{T}|a\rangle = |m|\exp(i\Psi) \\ &= \cos\left(\frac{\gamma_{\mathrm{bp}}}{2}\right)\exp\left(i\left(\varphi_{\mathbf{T}\mathrm{a}\to\mathrm{b}} - \frac{\Omega_{\mathrm{bp}}}{2}\right)\right). \end{aligned} \tag{15}$$

Taking into account Eqs. (7)-(9), the complex modulation can be written as

$$\begin{aligned} m = {} & \exp(i\varphi_1)\langle p|1\rangle\langle 1|a\rangle + \exp(i\varphi_2)\langle p|2\rangle\langle 2|a\rangle = \\ & = c_{1p}c_{a1}\exp\left(i\left(\varphi_1 - \frac{\Omega_{a1}+\Omega_{1p}}{2}\right)\right) \\ & + c_{2p}c_{a2}\exp\left(i\left(\varphi_2 - \frac{\Omega_{a2}+\Omega_{2p}}{2}\right)\right), \end{aligned} \tag{16}$$

where $c_{jk} = \cos(\gamma_{jk}/2)$, $(j,k = 1, 2, a, p)$, denote the amplitude terms of the corresponding projections. This expression can be factorized as

$$\begin{aligned} m = {} & \exp\left(i\left[\overline{\varphi} - \frac{\Omega_{a1p}+\Omega_{a2p}+2\Omega_{ap}}{4}\right]\right)\times\left\{c_{1p}c_{a1}\exp\left(i\left(-\omega - \frac{\Omega_{a1p}-\Omega_{a2p}}{4}\right)\right)\right. \\ & \left. + c_{2p}c_{a2}\exp\left(-i\left(-\omega - \frac{\Omega_{a1p}-\Omega_{a2p}}{4}\right)\right)\right\}, \end{aligned} \tag{17}$$

where the definitions $2\overline{\varphi} = (\varphi_2 + \varphi_1)$ and $2\omega = (\varphi_2 - \varphi_1)$ have been previously used, as well as the relations $\Omega_{anp} + \Omega_{ap} = \Omega_{an} + \Omega_{np}$, $n = 1,2$, derived directly from Eq. (8).

We can now define an angle 2Θ corresponding to the minor angle of the lune defined by the great arcs joining $|1\rangle$ and $|2\rangle$ and passing through $|a\rangle$ and $|p\rangle$ (Fig. 3(b)). This lune has a solid angle 4Θ. Similarly, the lune described by the action of the waveplate has a minor angle 2ω and a solid angle 4ω (upper light yellow lune in Fig. 3(b)). Therefore their subtraction defines a new lune with area $4(\Theta-\omega)$, as indicated in light red in Fig. 3(b). Note that $\Omega_{a2p} - \Omega_{a1p} = 4\Theta$. In addition, $\Omega_{a2p} + \Omega_{a1p}$ is equal to $2\Omega_{a\overline{a}\overline{p}p}$, where $\Omega_{a\overline{a}\overline{p}p}$ is defined in analogy to $\Omega_{a\overline{a}\overline{b}b}$ in Fig. 2(c). The latter is the spherical quadrangle defined by states $|a\rangle$, $|p\rangle$, $|\overline{a}\rangle$ and $|\overline{p}\rangle$. These last are defined by the intersection of the great arcs joining $|1\rangle$ and $|2\rangle$ and passing through $|a\rangle$ and $|p\rangle$, with the great circle perpendicular to the axis joining $|1\rangle$ and $|2\rangle$; see Fig. 3(c). Thus, using all these relations, Eq. (17) can be rewritten as

$$\begin{aligned} m &= \exp\left(i\left[\overline{\varphi} - \frac{\Omega_{a\overline{a}\overline{p}p}+\Omega_{ap}}{2}\right]\right)\times\left\{c_{1p}c_{a1}\exp(i(\Theta-\omega)) + c_{2p}c_{a2}\exp(-i(\Theta-\omega))\right\} = \\ &= \exp\left(i\left[\overline{\varphi} - \frac{\Omega_{a\overline{a}\overline{p}p}+\Omega_{ap}}{2}\right]\right)\times\left\{\cos\left(\frac{\gamma_{a1}-\gamma_{1p}}{2}\right)\cos(\Theta-\omega) + i\sin\left(\frac{\pi}{2} - \frac{\gamma_{a1}-\gamma_{1p}}{2}\right)\sin(\Theta-\omega)\right\} \end{aligned} \tag{18}$$

where we used the following relations $\cos(\gamma_{a2}/2) = \sin(\gamma_{a1}/2)$, $\cos(\gamma_{2p}/2) = \sin(\gamma_{1p}/2)$ and $\cos(\gamma_{1p}/2) = \sin(\gamma_{2p}/2)$. Note now the equivalence of the term inside the braces in the last line of Eq. (18) with the expression in Eq. (4) describing the projection between two states. This leads to the conclusion that this last term can be regarded as the projection of a state $\left|\theta = \omega, \varepsilon = \frac{\pi}{2} - \gamma_{a1}\right\rangle$ onto a state $\left|\theta = \Theta, \varepsilon = \frac{\pi}{2} - \gamma_{1p}\right\rangle$. This exactly corresponds to the shaded area in Fig. 3(d), with solid angle $\Omega_{p\overline{p}\overline{b}b}$ where we used that $\gamma_{a1} = \gamma_{1b}$. Therefore, we can rewrite Eq. (18) as

$$m = \cos\left(\frac{\gamma_{bp}}{2}\right)\exp(i\overline{\varphi})\exp\left(-i\frac{\Omega_{ap}}{2}\right)\exp\left(-i\frac{\Omega_{a\overline{a}\overline{p}p}+\Omega_{p\overline{p}\overline{b}b}}{2}\right) \tag{19}$$

Finally, let us use again Eq. (8) to note that $\Omega_{a\overline{a}\overline{p}p} + \Omega_{p\overline{p}\overline{b}b} = \Omega_{abp} + \Omega_{a\overline{a}\overline{b}b}$, so the modulation can also be written as

$$m = \cos\left(\frac{\gamma_{bp}}{2}\right)\exp(i\overline{\varphi})\exp\left(-i\frac{\Omega_{ap}}{2}\right)\exp\left(-i\frac{\Omega_{abp}+\Omega_{a\overline{a}\overline{b}b}}{2}\right) \tag{20}$$

This last representation is shown in Fig. 3(e), where the solid angles Ω_{abp} and $\Omega_{a\overline{a}\overline{b}b}$ have been shadowed. Note that the last exponential terms in Eqs. (19) and (20) correspond to the phases gained through an open loop of projections $|b\rangle\to|p\rangle\to|a\rangle$, but referred to the great circle perpendicular to the axis joining $|1\rangle$ and $|2\rangle$.

Eqs. (19) and (20) show two alternative ways to write the complex modulation obtained with polarization modulators. Note that the intensity modulation is given by $i = \cos^2(\gamma_{bp}/2)$. The term $\exp(i\overline{\varphi})$ can be dependant on the modulation characteristics of the modulator, but it does not depend on the selection of the states $|a\rangle$ and $|p\rangle$. On the contrary, the term $\exp(-i\Omega_{ap}/2)$ is fixed by the selection of states $|a\rangle$ and $|p\rangle$, but it is a constant phase which is not affected by the device modulation. The last exponential term in Eqs. (19) and (20) is the main relevant term in polarization modulation devices since it provides the only phase modulation term which depends both on the modulation characteristics of the device (its retardance and its principal axes variation) and the selection of the input and output transmitted states. Therefore, the phase modulation characteristics of the modulator can be controlled with the proper selection of the states $|a\rangle$ and $|p\rangle$, corresponding to the light illuminating the device and the state transmitted by the polarization detection system, respectively. Note that the decomposition of solid angles presented in Eq. (20) is especially useful when studying complex optical modulators, since it splits the action of modulators into different terms. On one hand, the Ω_{abp} term accounts for retardance variation (2ω), input polarizer and output analyzer polarizer states, while it is completely insensitive to neutral axes variation, if any. On the other hand, the $\Omega_{a\overline{a}\overline{b}b}$ term accounts for neutral axes variation phase effect, as well as input state and device retardance, while it is insensitive to the analyzer polarizer state location. The $\Omega_{a\overline{a}\overline{b}b}$ term becomes an extremely important phase factor when studying complex modulation devices, like TN-LCDs, since they present variations in the orientation of the neutral axes.

5. Example and experimental verification

In this final section, we present the application of the above presented method to evaluate the modulation produced by a parallel aligned (PAL) liquid crystal display in different polarization configurations. This type of polarization modulator is simple to analyze, since it acts as a programmable waveplate with fixed orientation of the principal axes, and where one eigenphase (corresponding to the ordinary axis) is maintained fixed, $\varphi_1 = \varphi_o$, whereas the other eigenphase $\varphi_2 = \varphi_e$ (corresponding to the extraordinary axis) can be modified via a voltage applied to the liquid crystal cell, which in turns is controlled via the gray level (g) addressed from a computer. Therefore, $\varphi_2 = \varphi_e(g)$, and the device has a controllable retardance $2\omega(g) = \varphi_e(g) - \varphi_o$.

In order to act as programmable phase plates, these devices are usually illuminated with linearly polarized light aligned along the extraordinary axis (orientation of the liquid crystal director). In our experiment we used a different scheme. We illuminated the display with linearly polarized light aligned at 45° with respect the ordinary neutral axis, in order to produce substantial changes in the emerging

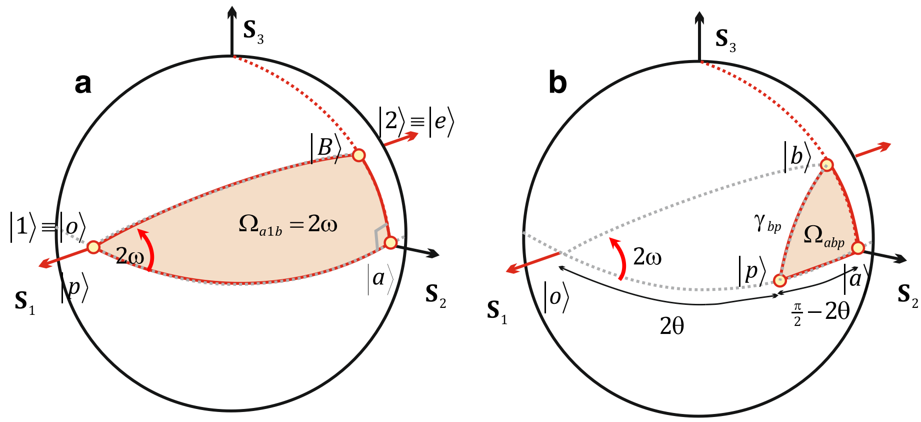

Fig. 4. Spherical triangles on the Poincaré sphere, which are useful to calculate the complex modulation produced by a parallel aligned liquid crystal display. Input linear polarization is selected along S_2 axis. (a) Spherical triangle used to calculate the phase gained after passing the display. (b) Spherical triangle used to calculate the phase upon projection onto an analyzer $|p\rangle$.

polarization states. We consider the ordinary axis coincident with the S_1 axis in the Poincaré sphere, and input polarization along the S_2 axis. In this situation, as the retardance ω increases, the emerging state describes the meridian starting at S_2. This configuration produces a notable simplification of the geometric analysis, since now the solid angle $\Omega_{a\bar{a}\bar{b}b}$ (Fig. 3(e)) vanishes.

The geometric calculation of the complex modulation can be done in the various methods described above. First, we can evaluate the phase $\varphi_{\mathbf{T}:a\rightarrow b}$ of the state $|B\rangle$ emerging from the display as a function of the retardance 2ω. This can be done according to the discussion in Section 3, for instance with Eq. (13). If we consider the eigenvector corresponding to the ordinary axis, then $\varphi_1=\varphi_o$, and the two involved solid angles are $\Omega_{a1b}=-2\omega$ and $\Omega_{ab}=0$ (see Fig. 4a). Therefore, the direct application of Eq. (13) leads to $\varphi_{\mathbf{T}:a\rightarrow b}=\varphi_o+\omega$. Note that the same results are easily obtained from Eq. (14) since $\Omega_{a\bar{a}\bar{b}b}=0$ and $\overline{\varphi}=\varphi_o+\omega$.

Now let us consider the projection of state $|b\rangle$ onto a polarizer $|p\rangle$. As a first simple example, we can assume the linear polarizer oriented along the direction of the ordinary axis, $|p\rangle=|o\rangle$ (Fig. 4(a)). In this case, the polarizer is selecting the polarization component where no phase modulation is produced versus the applied voltage, and therefore no phase variation with the retardance is expected. This is verified

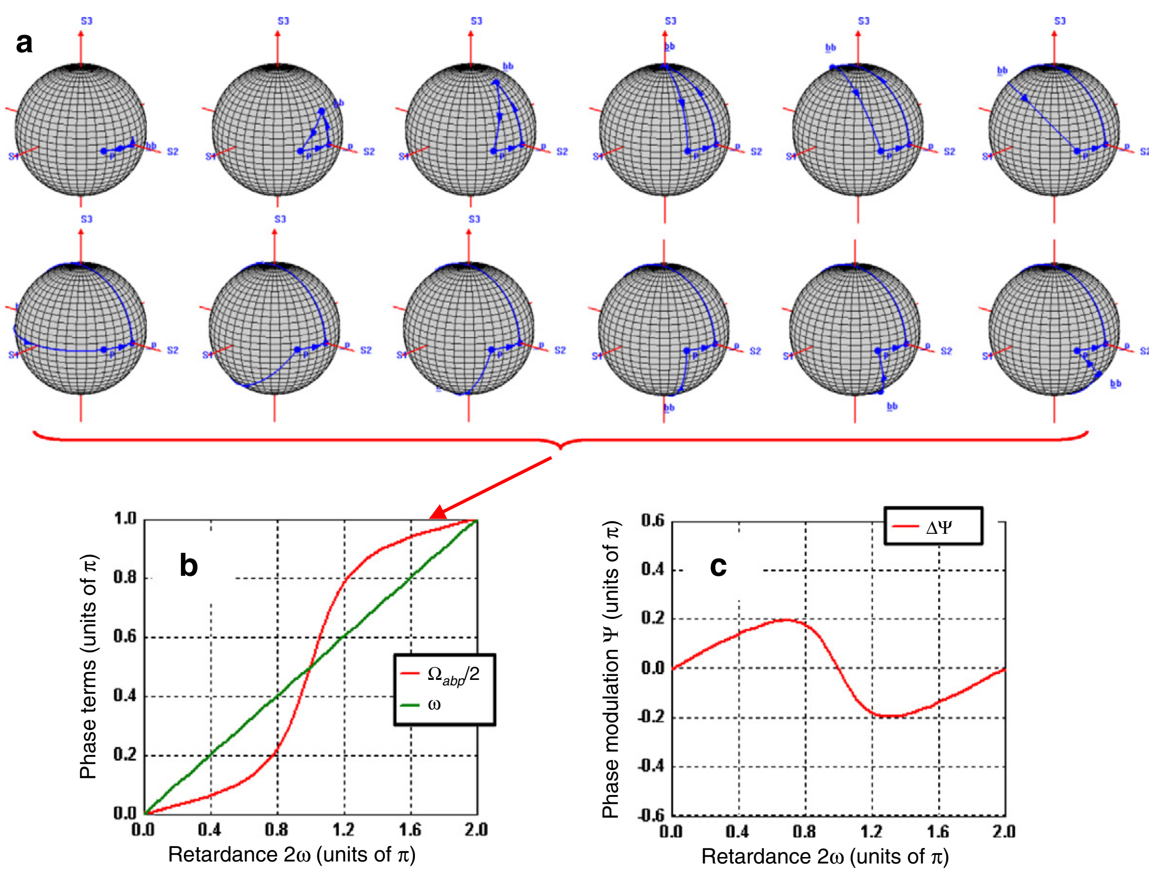

Fig. 5. Phase modulation for the case with the polarizer oriented in $\theta_p=30°$. (a) Geometric representation of the solid angle Ω_{abp} as the retardance 2ω increases from 0 to 360°. (b) Phase terms $\Omega_{abp}/2$ and ω versus retardance. (c) Phase modulation ΔΨ versus retardance.

since the projection $|b\rangle \rightarrow |p\rangle$ gives the solid angle $\Omega_{bp}/2 = -\omega$, thus having a total phase after the polarizer (Eq. (15)) $\Psi = \overline{\varphi} - \Omega_{bp}/2 = \varphi_o$, i.e., constant and independent of the retardance ω. A similar argument leads to a total phase $\Psi = \varphi_o + 2\omega$ when the polarizer is selected along the orientation of the extraordinary axis, $|p\rangle = |e\rangle$. In both cases the amplitude term is $|m| = 1/2$ for every value of ω. This results on obtaining a perfect phase-only modulation when $|p\rangle = |e\rangle$ and a constant transmission value when $|p\rangle = |o\rangle$.

More interesting is the analysis when the analyzer has an arbitrary orientation θ_p. In this case we can directly apply the method discussed in Section 4, Eq. (20). The amplitude term is given by $|m| = \cos(\gamma_{bp}/2)$. For this case $\Omega_{ap} = 0$ since $|a\rangle$ and $|p\rangle$ lie both in the equator (Fig. 4(b)), and also $\Omega_{a\bar{a}\bar{b}b} = 0$. Therefore, the total phase is given by $\Psi = \overline{\varphi} - \Omega_{abp}/2$. The relative phase modulation, understood as the relative phase difference between the phase Ψ for a given retardance 2ω with respect to the phase Ψ_0 for a null retardance, is given by

$$\Delta\Psi = \Psi - \Psi_0 = \omega - \frac{\Omega_{abp}}{2} \tag{21}$$

Note that the ω term is independent of the orientation of the polarizer. Thus, the changes in the phase modulation when changing the orientation of the polarizer are due to the variations in the solid angle Ω_{abp}. This is shown in Fig. 5(a), which represents how this solid angle grows as the value of ω increases. The spherical triangle $|a\rangle,|b\rangle,|p\rangle$ has been drawn in the Poincaré sphere as ω grows from 0° to 360° in steps of 30°. The orientation of the polarizer has been selected to be $\theta_p = 30°$. Fig. 5(b) shows the evolution of $\Omega_{abp}/2$ with the retardance for this case. For comparison, the term ω in Eq. (21) has been also included as half the lune defined by $|a\rangle,|b\rangle,|o\rangle$. The phase term $\Omega_{abp}/2$ shows a non-linear behavior with respect to the retardance, being its slope stiffer as the analyzer angle tends to $\theta_p = 45°$. Their difference $\Delta\Psi$ (Eq. (21)) is shown in Fig. 5(c). Also note that the intensity and phase modulation components can be related to the polarizer orientation θ_p and the retardance 2ω simply by applying spherical trigonometry relations in the $|a\rangle,|b\rangle,|p\rangle$ spherical triangle, leading to

$$i = |m|^2 = \frac{1}{2}\left(1 + \cos(2\omega)\sin\left(2\theta_p\right)\right), \tag{22a}$$

$$\tan\left(\Omega_{abp}\right) = \frac{\sin(2\omega)\cos\left(2\theta_p\right)}{\cos(2\omega) + \sin\left(2\theta_p\right)} \tag{22b}$$

Regarding solid angle definitions, one must accomplish the following rules in order to properly define the correct shapes and calculate their corresponding area:

- Their lateral arcs (in this case arcs $|a\rangle,|b\rangle$ and $|b\rangle,|p\rangle$) must always vary continuously when the device retardance varies in a continuous way. In other words, the arc lengths always increase or decrease continuously.
- No arc jumps are allowed, and consequently phase jumps are not described by spontaneous transitions of these arcs, but for fast arc orientation variations.

These rules have been used when depicting the shapes in Fig. 5(a) and when calculating their corresponding area. These rules were

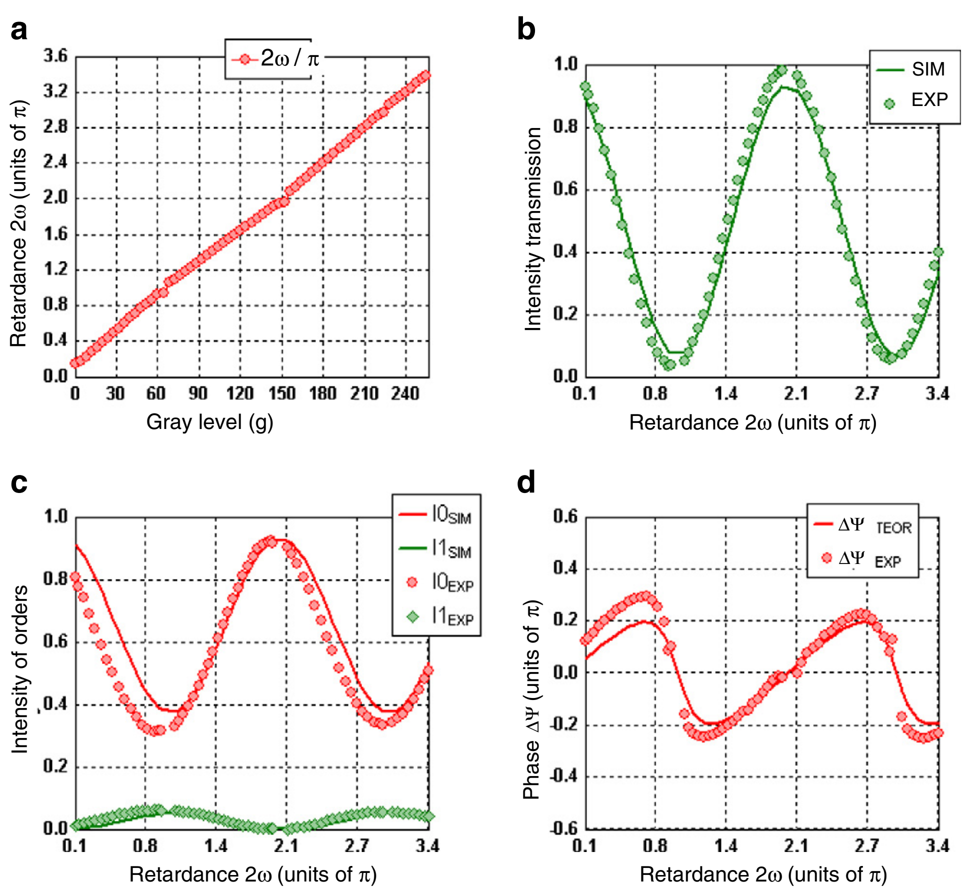

Fig. 6. Experimental results. (a) Retardance 2ω versus the addressed gray level (g). (b) Normalized intensity transmission. (c) Intensity of the zero and first diffraction orders generated by a binary grating. (d) Phase modulation ΔΨ.

found when comparing geometrical predictions with Jones calculus estimations, otherwise they do not match each other.

Regarding the non-linear behavior of phase modulation Ψ shown in Fig. 5(c), it is due to the geometrical shape defining $\Omega_{abp}/2$, and it is produced by rapid rotation of the arc from $|b\rangle$ to $|p\rangle$ (see Fig. 5(a)). This rotation presents the highest sensitivity for retardance $2\omega = \pi$, as verified by the high $\Omega_{abp}/2$ slope in Fig. 5(b). In addition, if we continuously approach $|p\rangle$ to $|a\rangle$, the total phase modulation tends to produce an abrupt π phase jump in the limit $|p\rangle \cong |a\rangle$. Similar phase jumps have been registered for the complex modulation of a TN-LCD system when it is inserted between parallel polarizers [21]. Another experiment showing phase jumps for an interferometric system using a rotating static waveplate is presented in ref. [3].

Finally, we have verified these results and experimentally measured the complex relative modulation in a liquid crystal display by means of a diffractive method presented in [22]. In our case, we used a parallel aligned nematic liquid crystal on silicon (LCOS) display from Hamamatsu, X10468-01 model, with 800×600 pixels. The voltage applied to the display is controlled through the gray level (g) addressed from a computer. First, a uniform screen is addressed in order to measure the intensity modulation $i(g) = |m|^2$ as a function of the addressed gray level g. Then, binary gratings are addressed to the display with one fixed gray level (g_0), and the second one changing in the complete range. From the intensity measured in the generated zeroth and first diffraction orders, the phase modulation $\Delta\Psi(g)$ can be obtained according to the method in ref. [22].

Fig. 6 collects the obtained experimental results. Fig. 6(a) shows the measured retardance 2ω versus the addressed gray level (g). It shows a linear retardance variation that exceeds 3π radians for the operating wavelength of 514 nm from an Ar ion laser. Fig. 6(b) shows the normalized intensity modulation $i(g)$ in the studied configuration (the input polarizer oriented at 45°, and the analyzer polarizer is oriented at 30° respect to the PAL ordinary axis). The solid line shows the prediction while the dots correspond to the experimental data, showing an excellent agreement. Fig. 6(c) shows the intensity of zeroth (I_0) and first (I_1) diffraction orders generated by a binary diffraction grating with a reference gray level g_0 (which we selected $g_0 = 150$ in order to correspond to a retardance equal to 2π) and a variable gray level g. These intensities are given by relations [22]:

$$I_0 = \frac{1}{4}\left(i_g + i_{150} + 2\sqrt{i_g i_{150}}\cos\Delta\Psi\right), \tag{23a}$$

$$I_1 = \frac{1}{\pi^2}\left(i_g + i_{150} - 2\sqrt{i_g i_{150}}\cos\Delta\Psi\right), \tag{23b}$$

Again, solid lines and dots correspond to the predictions and the experimental data, respectively, and show a very good agreement. Finally, Fig. 6(d) shows the phase modulation $\Delta\Psi(g)$ derived according to the method in [22], together with the prediction obtained from the geometrical analysis, which shows good agreement as well.

6. Conclusions

In summary, we have presented a method to geometrically evaluate the complex response of polarization systems, based on the Pancharatnam connection on the Poincaré sphere. This work contributes to demonstrate that the Poincaré sphere provides full information for both amplitude and phase modulation determination in optical modulators based on the variation of the optical properties of wave plates. The proposed geometrical analysis completes previous ones, especially those in refs. [9–11], by considering polarization states emerging from the modulator different from the input state, and therefore describing non-closed loops on the Poincaré sphere.

The presented analysis can be a useful tool to understand the physical insights of the complex (amplitude and phase) modulation in polarization optical modulators, especially for programmable liquid crystal wave plates. This method can provide a valuable and systematic tool to analyze the origin of several phenomena, like non-linear phase modulation effects, increased phase modulation [17] or even more complex physics problems. Here, it has been applied to evaluate the complex modulation of a parallel aligned liquid crystal display, showing a very good agreement between experiment and the predicted result.

Acknowledgements

José Luis Martínez Fuentes is deeply grateful to PhDs Antonio Martínez García and Alfonso Salinas Castillo, his family, as well as all the friends who have supported him all along these years. This work belongs to all of them. JLMF also acknowledges a grant from Conselleria d'Educació i Ciència from Generalitat Valenciana. This work received financial support from Ministerio Ciencia e Innovación from Spain (ref. FIS2009-13955-C02-02), and from Conselleria d'Educació i Ciència from Generalitat Valenciana (ACOMP/2011/112). Jorge Albero acknowledges the financial support from Ministerio de Educación through the Programa Nacional de Movilidad de Recursos Humanos del Plan Nacional de I+D+i 2008–2011.

References

[1] S. Pancharatnam, Proceedings Industrial Academy Science A 44 (1956) 247.
[2] M.V. Berry, Journal of Modern Optics 34 (1987) 1401.
[3] R. Bhandari, Physics Letters A 180 (1993) 15.
[4] R. Bhandari, Current Science 67 (1994) 224.
[5] P. Hariharan, in: E. Wolf (Ed.), Progress Optics, 48, Elsevier, 2005, p. 149.
[6] Z. Bomzom, V. Kleiner, E. Hasman, Optics Letters 26 (2001) 1424.
[7] L. Marrucci, C. Manzo, D. Paparo, Applied Physics Letters 88 (2006) 221102.
[8] Y. Aharomov, J. Anandan, Physical Review Letters 58 (1987) 1593.
[9] H. Schmitzer, S. Klein, W. Dultz, Journal of Modern Optics 45 (1998) 1039.
[10] J. Courtial, Optics Communication 171 (1999) 179.
[11] P. Kurzynowski, W.A. Wozniak, M. Szarycz, Journal of the Optical Society of America A 28 (2010) 475.
[12] T. van Dijk, H.F. Schouten, W. Ubachs, T.D. Visser, Optics Express 18 (2010) 10796.
[13] T. van Dijk, H.F. Schouten, T.D. Visser, Journal of the Optical Society of America A 27 (2010) 1972.
[14] J.C. Gutiérrez-Vega, Optics Letters 36 (2011) 1143.
[15] J.A. Davis, P. Tsai, D.M. Cottrell, T. Sonehara, J. Amako, Optical Engineering 38 (1999) 1051.
[16] M.M. Sánchez-López, P. García-Martínez, A. Martínez-García, I. Moreno, Journal of Optics A: Pure and Applied Optics 11 (2009) 015507.
[17] J.L. Martínez, I. Moreno, J.A. Davis, T.J. Hernández, K.P. McAuley, Applied Optics 49 (2010) 5929.
[18] V. Durán, J. Lancis, E. Tajahuerce, V. Climent, Journal of Display Technology 3 (2007) 41883.
[19] V. Ramírez-Sánchez, G. Piquero, Óptica Pura y Aplicada 40 (2007) 87.
[20] J. Nicolás, J. Campos, M.J. Yzuel, Journal of the Optical Society of America A 19 (2002) 1013.
[21] K. Lu, B.E.A. Saleh, Optical Engineering 29 (1990) 240.
[22] Z. Zhang, G. Lu, F.T.S. Yu, Optical Engineering 33 (1994) 3018.